Plume Characteristics and Liquid Circulation in Gas Injection through a Porous Plug

P.E. ANAGBO and J.K. BRIMACOMBE

Various forms of plumes have been identified following the injection of air at different rates through a porous plug into water contained in a ladle-shaped vessel. Discrete bubbles form at the plug and rise uniformly through the column of liquid at gas flow rates up to 14 $cm^3/s\ cm^2$ of plug surface; at higher flow rates, groups of bubbles increasingly coalesce into larger gas pockets, and beyond about 40 $cm^3/s\ cm^2$, the gas globes are large enough to cover the entire plug surface before detachment and gradual disintegration as they rise through the body of liquid. The gas fraction, as well as bubble frequency, bubble velocity, and bubble size, have been measured in the various dispersion regimes by means of an electroresistivity probe. The radial distributions of gas fraction and bubble frequency are approximately bell-shaped about the axis of flow, and the reduced values are close to Gaussian functions of the reduced radial distance from the axis. The gas fraction along the axis has been correlated to the reduced height of the plume; it increases with decreasing distance above the plug and with increasing gas flow rate. The axial bubble frequency shows a decrease in the vicinity of the plug with the onset of bubble coalescence, but the values of the frequencies at all gas injection rates converge to about 12 s^{-1} toward the surface of the bath. The mean bubble velocity increases with increasing flow rate but drops once coalescence is fully established. Conversely, there is a sudden increase in the mean bubble diameter with the onset of coalescence. The axial and radial components of the velocity of the liquid surrounding the plume have been measured by means of a Laser-Doppler Velocimeter (LDV), and the results show that the circulation patterns are identical, irrespective of the dispersion regime. The axial flow which is upward in the vicinity of the plume decreases in magnitude with increasing radial distance, ultimately reversing to an increasing downward flow beyond a certain distance from the plug axis. Similarly, the radial flow which is outward from the plume near the liquid surface decreases steadily with depth and eventually reverses to an inward flow at a depth independent of the gas injection rate. The profiles of the axial velocities are almost sigmoidal, except in the coalescence regime, where the effect of turbulence is profound at the upper liquid layers. The radial liquid velocities are generally small relative to the axial components, only about one-fifth as large, considering the maximum average values.

I. INTRODUCTION

THE design and performance of porous plugs for the injection of purging and homogenizing gases into molten metals have recently been reviewed.[1,2] A particularly important application of the plug is in the ladle treatment of steel, where porous refractory elements are assembled into the bottom wall of the ladle as a means of introducing inert gases into the melt for flushing out inclusions and homogenizing temperature and composition prior to casting.[3–8] Similar gas injection arrangements exist for desulfurization and recarburization of iron[9,10,11] and also for steelmaking by the lance bubbling equilibrium (LBE) process.[6] In the treatment of nonferrous metals, porous plugs are commonly used in the gaseous refining of anode copper[12,13] and for the degassing and stirring of aluminum melts for improved casting.[14]

In metal refining practice, the porous plug has been shown to be more efficient than the tuyere in gas utilization[15] and more effective than the lance in ladle operations.[4] Nevertheless, not very much is known about the physical interaction of gas and liquid in porous plug injection to properly account for the observed superior refining performance of the porous plug. In their work on gas bubble beds, Houghton *et al.*[16] related the average pore diameter, δ, of a glass or steel porous plug to the pressure drop, ΔP, across the plug and the surface tension, σ, of the liquid in the form

$$\delta = \frac{4\sigma}{\Delta P - \Delta P_f} \qquad [1]$$

where ΔP_f is the frictional component of the pressure drop. A more practical index of the resistance to gas flow through the plug is the permeability, ζ, which can be determined from the expression[8]

$$\zeta = \frac{\nu Q h}{A \Delta P} \qquad [2]$$

where ν is the kinematic viscosity of the gas, h is the height of the plug of cross-sectional area A, and ΔP is the pressure drop across the plug under a gas flow rate, Q. It has been shown in laboratory model studies that the gas flow rate through a porous plug increases linearly

P.E. ANAGBO, Associate Professor, is with the Department of Metallurgical Engineering, University of Lagos, Lagos, Nigeria. J.K. BRIMACOMBE, Stelco/NSERC Professor and Director, is with the Centre for Metallurgical Process Engineering, The University of British Columbia, Vancouver, BC V6T 1W5, Canada.

Manuscript submitted October 18, 1989.

with increasing injection pressure but only for low values of permeability.[16]

Houghton *et al.*[16] also investigated the dispersion of gas injected into liquid by means of a porous plug and described the formation of fine bubbles, which were oblate spheroidal in shape, with the bubble size well correlated by means of a probability function. No influence of plug permeability on the size and density distributions of the bubbles was reported, but in a subsequent study, Koide *et al.*[17] demonstrated the effects of plug porosity (ε), pore size (δ), liquid density (ρ), and surface tension (σ) on the average bubble diameter, in the form of a correlation:

$$d = K\left(\frac{\mathrm{Fr}}{\mathrm{We}^{1/2}}\right)^{n}\left(\frac{\sigma\delta}{\rho g}\right)^{1/3} \quad [3]$$

where

$$\mathrm{Fr} = \frac{u^2}{\varepsilon^2 g\delta} \quad [4]$$

and

$$\mathrm{We} = \frac{u^2\delta P}{\varepsilon^2\sigma} \quad [5]$$

u being the superficial gas velocity. The coefficient K and exponent n showed transitions in value, on the basis of which two regimes of gas dispersion were identified in the range of experimental conditions. Baxter and Wraith[18] studied a scaled-up model of porous plug injection and observed quiescent columns of discrete air bubbles in water at gas flow rates up to 16 $cm^3/s\ cm^2$ of the plug surface, bubble column pulsation between 16 and 30 $cm^3/s\ cm^2$, incipient coalescence of bubbles between 30 and 38 $cm^3/s\ cm^2$, and bubble "blanketing" of the entire plug surface at gas flow rates above 67 $cm^3/s\ cm^2$. A gas fraction of 0.7 was postulated for the bubble regime, assuming close-packed bubble spheres, in predicting the onset of coalescence. Similarly Goyal *et al.*[12] injected air through an industrial porous plug into water and observed a regime of discrete bubbles at flow rates up to 15 $cm^3/s\ cm^2$, with coalesced bubbles beyond 25 $cm^3/s\ cm^2$; the discrete bubble dispersion was a plume of fine bubbles rising in water with an upwardly expanding angle of about 20 deg.

The circulation in a ladle during porous plug injection was recently studied by Johansen *et al.*[19] on the basis of an air-water model. Axial and radial mean and fluctuating velocities were measured in both the plume and the surrounding liquid phase by means of a Malvern 6200 Laser Photon Correlation Velocimeter; it was found that the flow field in a gas-stirred ladle is complicated, with the bubbles contributing to the production of turbulence. The velocities depend on gas flow rate, bubble size, and ladle geometry, but no similarity was established between velocity profiles at different gas flow rates. The measurements were in good agreement with a mathematical model presented by Johansen and Boysan[20] who combined the equations of continuity and conservation of momentum of the liquid phase with the equation of motion of the bubbles, allowing for bubble group interaction.

Sahai and Guthrie[21] argued that flow recirculation in industrial furnaces or ladles is independent of whether the gas source is a nozzle, tuyere, or porous plug. They further estimated that the gas fraction in such systems would only range from 0.02 to 0.1, and by equating the energy supplied by the rising bubbles to turbulent energy dissipation in the bath, they predicted the plume velocity (U_p) in terms of the gas flow rate (Q), the liquid depth (L), and the radius of the cylindrical vessel (R); thus,

$$U_p = C\frac{Q^{1/3}L^{1/4}}{R^{1/3}} \quad [6]$$

A mathematical model[22] based on the prescribed plume dimensions and velocities, as well as gas fractions, was shown to predict axial and radial liquid velocities in agreement with experimental measurements. However, data were obtained only for injection through the nozzle. Similarly, Stapurewizc and Themelis[23] also found that the mixing time of a bath is independent of whether a porous plug or a tuyere was used to introduce the gas, and at what injection velocity, for a given gas flow rate. However, the gas absorption rate was much higher for the porous plug at low gas flow rates, where the bubbles were finer and the interfacial areas much higher, than for the tuyere.

Thus, so far, the performance of the porous plug has been assessed on the basis of estimated bulk properties of the plume generated above the plug in operation. By implication, it has been assumed that the properties of the dispersion are uniformly distributed throughout the plume and, indeed, that the mechanism of plume formation is not affected by changes in operating conditions. The present work is designed to actually determine the spatial distributions of the vital properties of the plume above the plug: gas fraction, bubble size, bubble frequency, and bubble velocity, as well as the induced velocity components in the liquid surrounding the plume. These properties have been obtained for three different values of gas injection rate which have been shown to correspond to different mechanisms of plume formation.

II. EXPERIMENTAL

The experiments in plume characterization were performed using a 1/6th-scale model of a 150-tonne ladle. The apparatus consists of a 500-mm-diameter cylindrical tank of PLEXIGLAS* containing deionized water to a depth of 400 mm and equipped with a porous plug assembly located at the center of the base, as shown in Figure 1(a). The porous element is a fritted glass disc, 60-mm in diameter and 5-mm thick, closely fitted in a PLEXIGLAS holder assembled with sealing O-rings. It was found necessary to introduce a distributor plate just upstream of the porous disc to ensure a uniform flow of gas over the cross-sectional area of the plug. The schematic diagram of the plug assembly is shown in Figure 1(b), and the effective depth of water was measured from the surface of the porous element. A

*PLEXIGLAS is a trademark of Rohm & Haas Company, Philadelphia, PA.

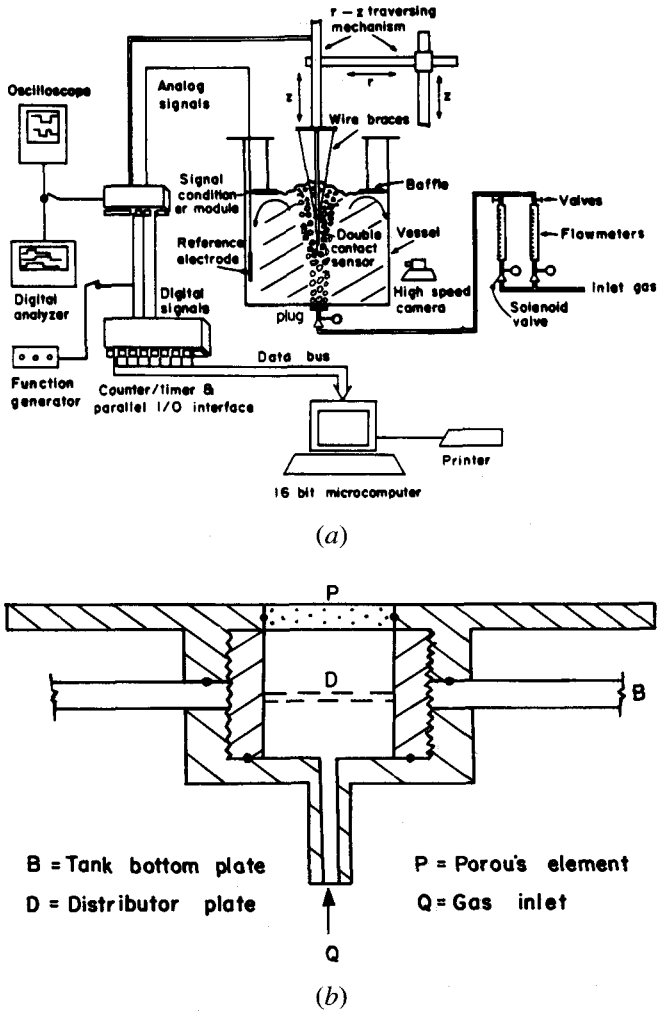

Fig. 1—Schematic of the experimental apparatus: (*a*) cylindrical tank equipped with a porous plug and electroresistivity sensor and (*b*) details of the porous plug assembly.

PLEXIGLAS ring baffle with a 496-mm OD and 300-mm ID was positioned some 3 mm above the static level of the bath to prevent bath slopping, especially at high gas injection rates. Compressed air was connected to the porous plug across an air filter, a solenoid control switch, and a bank of rotameters equipped with pressure gauges and gate valves.

Measurements of gas fraction, bubble frequency, bubble axial diameter, and bubble velocity were obtained by means of a double-contact electroresistivity probe developed by Castillejos and Brimacombe.[24] The connection of the probe to a microcomputer across signal-conditioning circuits for data acquisition is as shown schematically in Figure 1. Once the water bath was made electrically conductive by introducing an adequate dose of acid, it was possible to monitor the dwell time of any gas pocket arriving at either tip of the probe. Measurements were made for a sample size of 800 bubbles at any position in the plume once the probe was located by means of the *z-r* traversing carriage of the probe.

Liquid velocity measurements in the bath surrounding the plume were made by means of a Laser-Doppler velocimeter (LDV); it was a TSI System 9100-3, based on a 15 mW He-Ne laser with matching optical and photomultiplier facilities, to make it applicable to both the backscatter and forward scatter light collection methods. The velocimeter was mounted on an automatic traversing fixture linked to an APPLE IIe* microcomputer, which was also used for data collection. The liquid velocity was obtained in the axial and radial components by rotating the beamsplitter through an angle of 90 deg with the measurement being in the direction perpendicular to the optical axis. Each mean velocity component was computed from a sample size of 512 readings, based on a beam spacing of 22 mm and a focusing half angle corrected for air-PLEXIGLAS-water refraction.[25]

*APPLE IIe is a trademark of Apple Computer, Inc., Cupertino, CA.

In a design to overcome the problem of laser beam deflection at the curved surface of the cylindrical tank, an octagonal tank was constructed based on a 500-mm square container, as shown in Figure 2. The values of liquid velocity obtained in a preliminary test along various radial directions in the octagonal tank were found to be identical beyond the close vicinity of the wall; hence, the octagonal tank was adopted as a finite element equivalent[26] of the cylindrical vessel. The bath depth was maintained at 400 mm, and the water was seeded by doping with styrene spheres which were uniformly distributed in the water bath and thus monitored the local water current by reflecting the projected laser beams.

The experiments were performed at room temperature

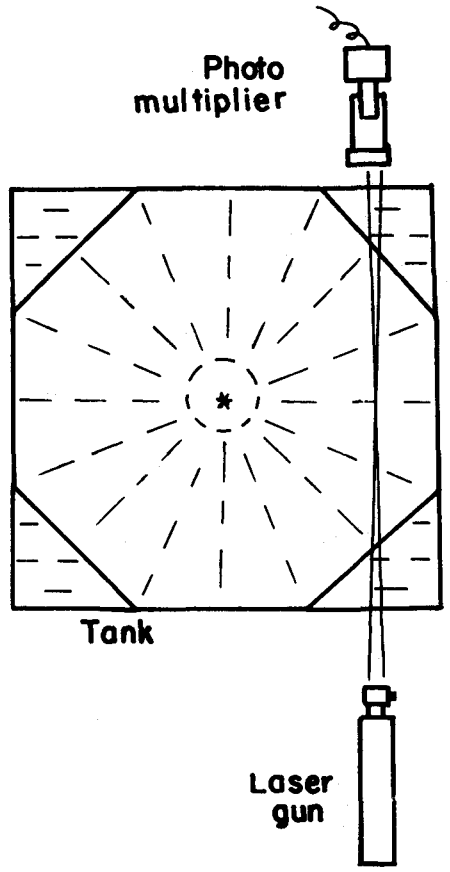

Fig. 2—Experimental facilities for the Laser-Doppler measurements.

and for three different gas flow rates: 200, 600, and 1200 Ncm^3/s. The injection rates were selected to span the various forms of plume dynamics as observed in a preliminary test and correspond to specific injection rates of 8.5, 25.3, and 50.5 $cm^3/s\ cm^2$, respectively.

III. RESULTS AND DISCUSSION

A. *Gas Dispersion Modes*

It is readily observed in a transparent bath that the plume above the porous plug shows certain peculiarities corresponding to different ranges of gas injection rate. The dispersion of the injected gas is in the form of small discrete bubbles at low injection rates, but the bubbles begin to coalesce with increasing gas flow rate, first in small bunches interspersed with discrete bubbles and, finally, as one large gas packet enveloping the entire surface of the plug. The three different modes of dispersion are shown in Figure 3. Bubble coalescence has a direct bearing on bubble frequency (and size) spectrum; thus, the variation in axial bubble frequency with increasing gas injection rate has been used as an indication of the changes in the modes of gas dispersion above the plug. Figure 4 shows the results obtained for various heights of the probe above the plug, with the effects of the changes in the dispersion modes being most profound at the probe location nearest the plug surface.

The axial bubble frequency increases with increasing gas flow rate up to about 8 $cm^3/s\ cm^2$ of the plug surface. This range corresponds to the development of the discrete bubble regime at the plug, and the increasing bubble frequency can be attributed to the progressive activation of dormant pores in the plug with increasing gas flow rate. The discrete bubble mode is fully established between about 8 and 14 $cm^3/s\ cm^2$, as indicated by the stable value of the axial bubble frequency. Thereafter, the bubbles begin to cluster and coalesce in small pockets, leading to a reduction in bubble frequency. The coalescence phenomenon gradually increases in intensity up to about 40 $cm^3/s\ cm^2$, by which stage the bubble frequency has decreased to a stable low value, signifying an established coalescence regime. Visual observation shows that the bubbles forming at the plug in this regime fuse into one large packet which envelopes the entire plug surface but starts breaking up as soon as it lifts off from the plug. The critical gas flow rate of 14 $cm^3/s\ cm^2$ between the regimes of discrete bubbling and incipient coalescence is in close agreement with the values of 15 and 16 $cm^3/s\ cm^2$ observed by Goyal *et al.*[12] and Baxter and Wraith,[18] respectively. However, their differing estimates of 25 and 67 $cm^3/s\ cm^2$, respectively, for the full development of the coalescence regime also differ from the measured value of 40 $cm^3/s\ cm^2$.

The measurements of axial bubble frequency obtained at locations more distant from the porous plug also confirm the gradual development of the discrete bubble regime. However, the pronounced effect of bubble coalescence in the vicinity of the plug becomes attenuated toward the surface of the bath. In general, the axial bubble frequency at a given gas flow rate decreases with distance above the plug, understandably due to the expanding geometry of the plume with continuous liquid entrainment into the two-phase zone.

In several applications of the porous plug, the aim is to produce a dispersion of discrete bubbles for enhanced interfacial area for effective transfer processes. Hence, the operational range between 8 and 16 $cm^3/s\ cm^2$ would be optimal in producing the maximum density of discrete bubbles without the incidence of coalescence into large

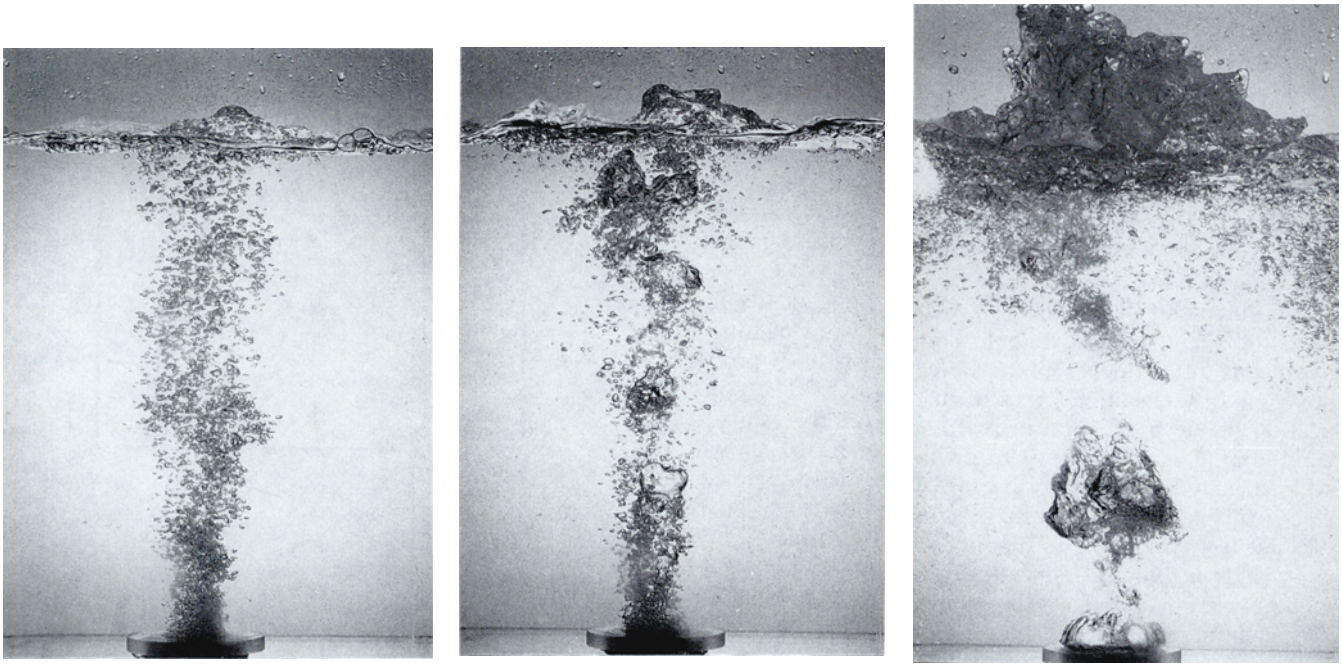

(*a*) (*b*) (*c*)

Fig. 3—Modes of gas dispersion in porous plug injection: (*a*) discrete bubbles, (*b*) incipient coalescence, and (*c*) coalescence.

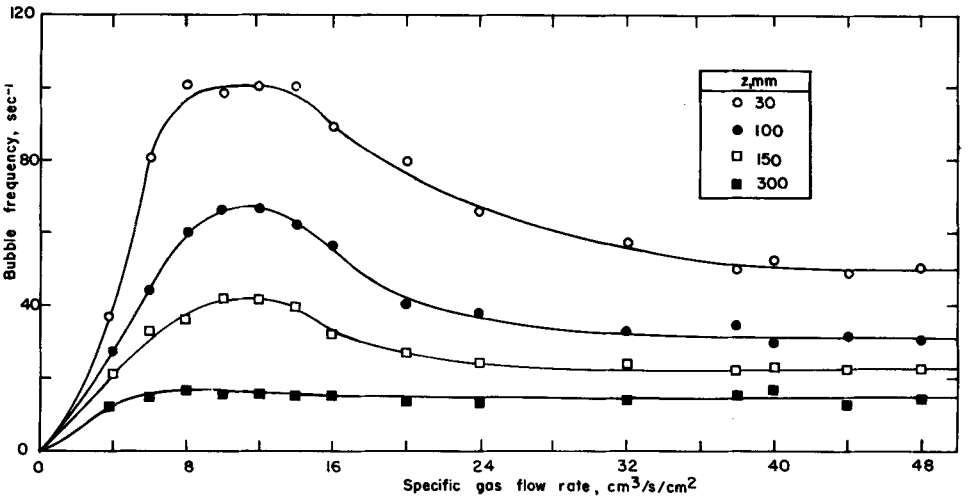

Fig. 4—Variation of bubble axial frequency with specific gas flow rate at various heights above the plug.

packets, provided that gas discharge behavior is reasonably similar in the model and real systems.

B. *Gas Fraction Profiles*

The fraction of observation time during which a given location in the plume is occupied by the gas phase has been measured at six different heights above the plug surface and at various radial positions to construct the gas fraction profiles for the three different gas flow rates, as shown in Figure 5. A consistent symmetry was observed in all of the profiles, which have therefore been represented by half-section maps.

In general, the gas fraction profiles are approximately bell-shaped, with the maximum values along the axis of the plug. At a given gas flow rate, the axial gas fraction decreases with increasing distance above the plug, which is expected as more and more liquid is entrained into the plume. The effect of increasing the gas flow rate is twofold; the bell-shaped profiles become wider and the axial gas fractions relatively larger at all levels above the plug.

The minimum distance above the plug at which consistent data could be obtained about the plume at all of the flow rates considered was about 30 mm. Below this level, the bubbles were too clustered or coalesced (at the higher injection rates) to allow accurate measurements

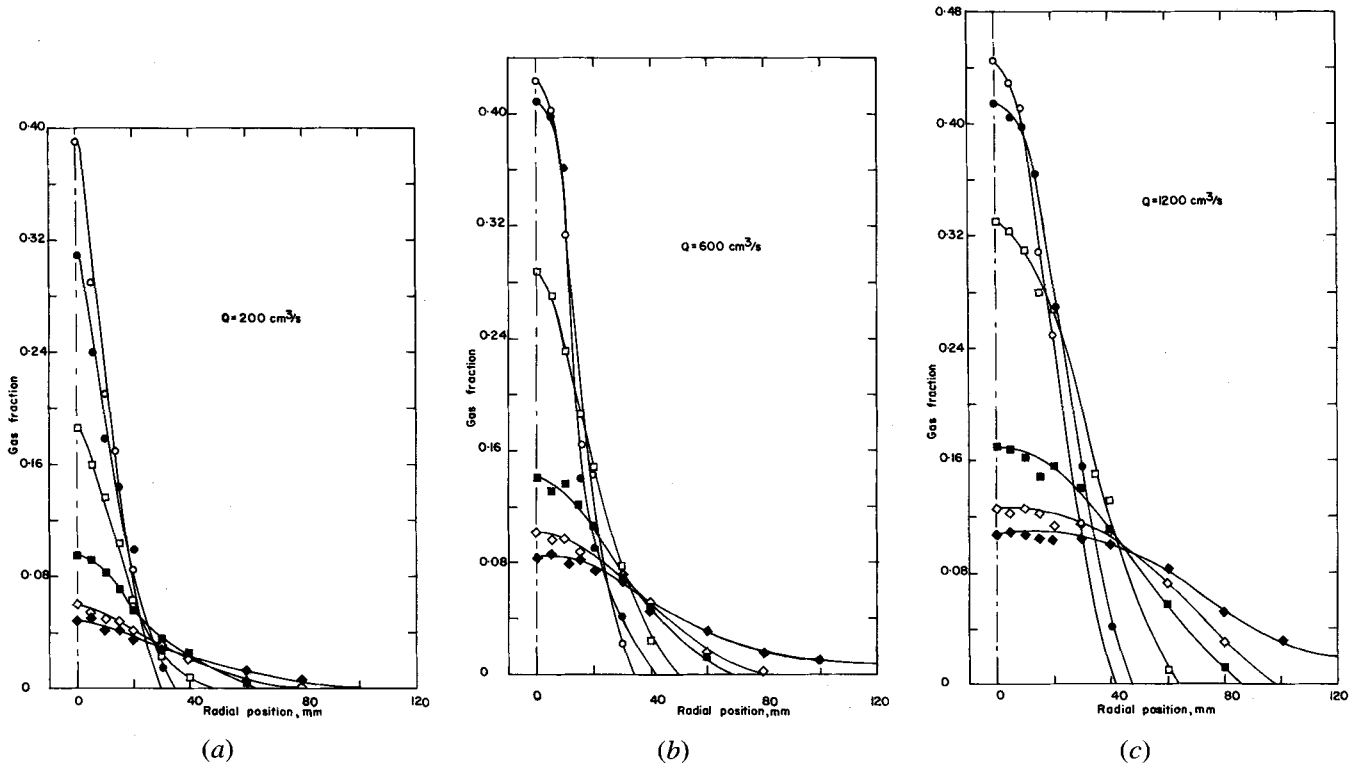

Fig. 5—Gas fraction profiles: (*a*) 200 cm³/s, (*b*) 600 cm³/s, and (*c*) 1200 cm³/s.

with the probe. A similar effect was reported by Castillejos and Brimacombe[24] for dispersion above the plate orifice, where they observed that the plume only became fully developed some 50 mm above the orifice. At 30 mm above the plug, the axial plug fractions were 0.39 at a gas injection rate of 200 cm^3/s, 0.42 at 600 cm^3/s, and 0.44 at 1200 cm^3/s. Even the maximum gas fraction of 0.39 in the bubble regime is much lower than the value of 0.7 which has been postulated by Baxter and Wraith[18] on the basis of close-packed bubble spheres.

Similarly, the maximum distance above the plug at which measurements could be made in the plume without interference from surface waves was about 380 mm. At that level, the axial gas fraction had dropped to 0.05 at 200 cm^3/s, 0.08 at 600 cm^3/s, and 0.1 at 1200 cm^3/s. These minimum values fall within the range of 0.02 to 0.1 estimated by Sahai and Guthrie[21] as the average gas fractions in industrial ladles. As shown in Figure 6, the axial gas fractions at the various levels' heights between the two extreme levels and for the three values of the gas flow rate can be well correlated in terms of a reduced distance involving the axial height of the plume above the plug and the gas flow rate; thus,

$$\alpha_0 = 0.71\left[\frac{z}{(Q^2/g)^{0.2}}\right]^{-0.9} \qquad [7]$$

The variation of the reduced gas fraction, α/α_0, with the reduced radial position, $r/r_{\alpha_0/2}$, is approximately Gaussian, as shown in Figure 7. A similar result was also obtained for the fully developed plume at a plate orifice.[27]

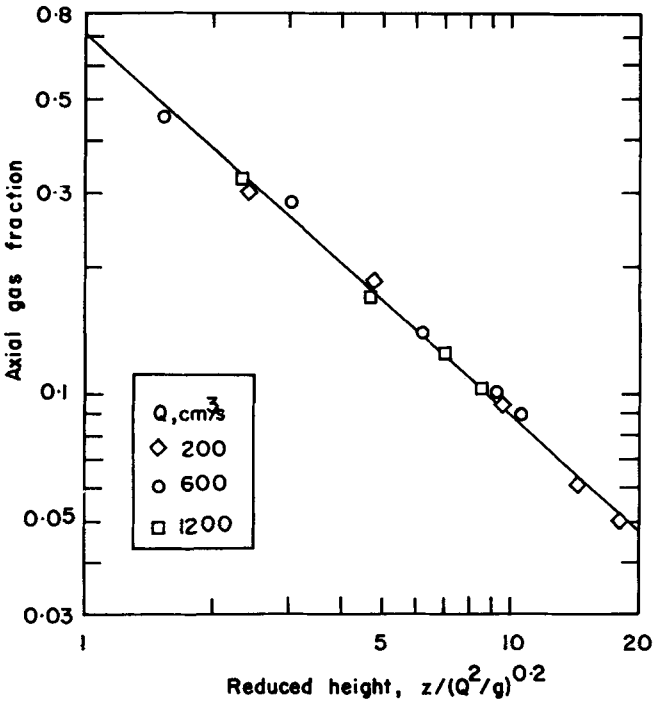

Fig. 6—Correlation of axial gas fraction with reduced height of the plume.

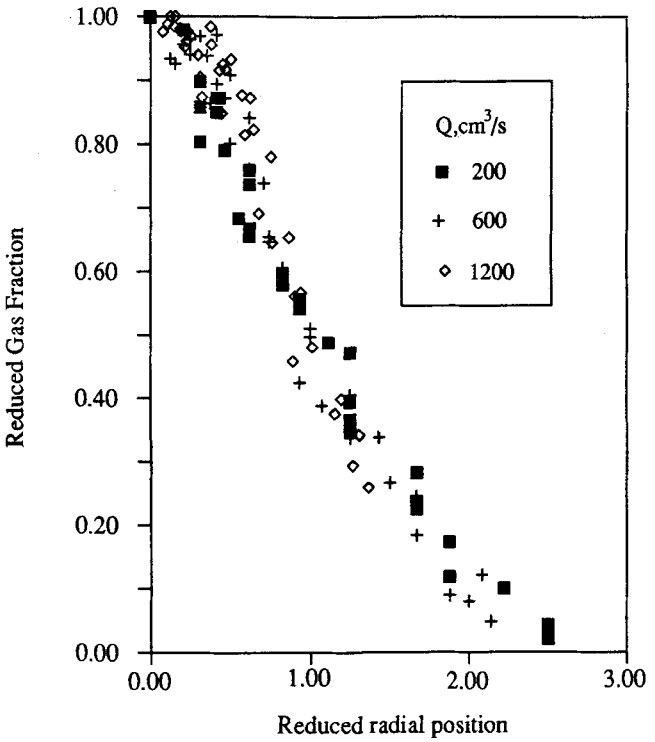

Fig. 7—Variation of reduced gas fraction with reduced radial position.

C. *Bubble Frequency Profiles*

The radial distributions of bubble frequencies at various heights above the porous plug are similar to those of the corresponding gas fractions in many respects. The bubble frequency profiles are still generally bell-shaped, as seen in Figure 8, and the axial bubble frequency at a given gas injection rate decreases with increasing height above the plug. The bubble frequency curves at a given height above the plug are also increasingly wider with increasing gas flow, as was the case with the gas fraction profiles.

The bubble frequency profiles, however, show clearly that the value of the axial bubble frequency at the deeper levels decreases when the gas flow rate is increased from 200 to 600 cm^3/s, and even more appreciably with a further increase to 1200 cm^3/s. The observation is consistent with the manifestations of incipient bubble coalescence around 600 cm^3/s and full coalescence at the plug in the region of 1200 cm^3/s. With coalescence, large gas packets are formed but at the expense of a number of the small bubbles. It was this principle of the variation in axial bubble frequency with gas flow rate in the vicinity of the plug which was applied in identifying the different gas dispersion regimes in Figure 4 above.

Apparently, the effect of bubble coalescence on the axial bubble frequency does not persist toward the surface of the bath, suggesting that the gas envelopes formed at the surface of the plug have largely disintegrated in rising through the bath. Indeed, at the height of 380 mm, close to the bath surface, the axial bubble frequency has a more or less uniform value of 10 to 12 s^{-1} for all of the dispersion regimes.

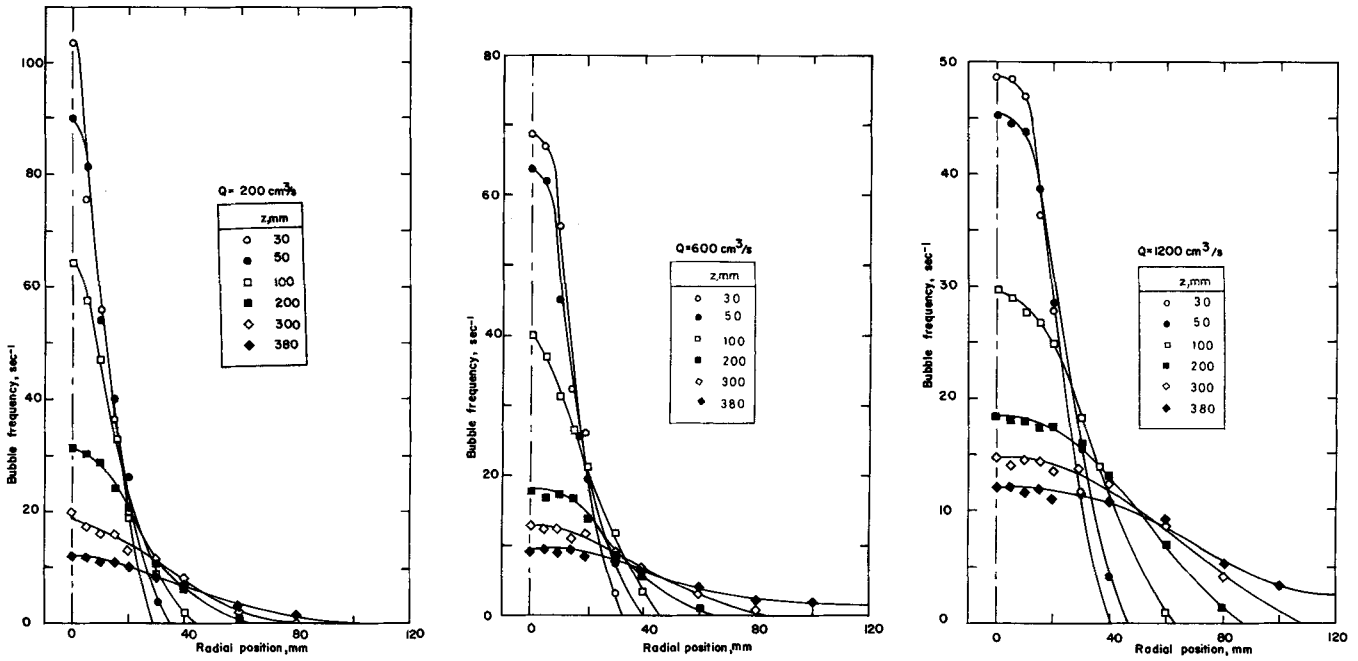

Fig. 8—Bubble frequency profiles: (*a*) 200 cm^3/s, (*b*) 600 cm^3/s, and (*c*) 1200 cm^3/s.

The variation of the reduced bubble frequency, f/f_0, with the reduced radial distance, $r/r_{f_0/2}$, is shown in Figure 9. It bears a striking similarity to the variation of the corresponding reduced gas fraction and can also be approximately described by a Gaussian function.

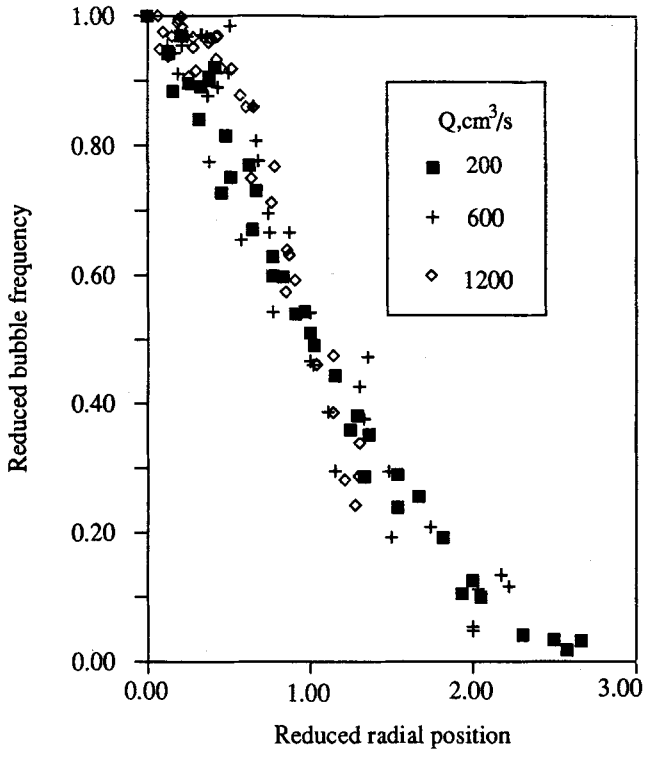

Fig. 9—Variation of reduced bubble frequency with reduced radial position.

D. *Bubble Velocity Profile*

The distributions of the rising velocities of the bubbles are shown in Figure 10. In general, the velocity distributions are symmetrical about the axis of the plug and decrease with increasing height above the plug and increasing radial distance from its center. For instance, at a gas flow rate of 200 cm^3/s, the axial bubble rise velocity decreases from about 1.05 m/s at the height of 50 mm above the plug to about 0.72 m/s at the height of 380 mm, 20 mm below the static surface. The radial gradient of the velocity is steeper deep in the plume than toward the surface, which reflects the high initial attenuating effects of gas-liquid momentum transfer in the plume. Consequently, while the bubble velocity at 50 mm above the plug drops from 1.05 m/s at the axis to 0.81 m/s over a radial distance of only 20 mm, there is a more gentle decrease in velocity at the height of 380 mm, from 0.72 m/s at the axis to 0.65 m/s over a radial distance of 40 mm.

The effects of gas flow rate, Q, on the bubble rise velocity depend on the operative mode of gas dispersion. Between discrete bubbling at 200 cm^3/s and incipient coalescence at 600 cm^2/s, ther bubble velocities increase with increasing gas flow rate. Thus, the corresponding mean axial bubble velocity at 600 cm^3/s ranges from 2.07 m/s at 50 mm above the plug to 1.23 m/s at the height of 380 mm. The increase in velocity is expected, considering the increased kinetic energy of the injected gas which, for single orifice injection, results in bubble velocities[28] proportional to $Q^{0.2}$. Once coalescence is established, however, the bubble rise velocity is decreased, especially in the vicinity of the plug. Thus, at 1200 cm^3/s, the mean bubble rise velocity 50 mm above the plug is only 1.41 m/s or barely 68 pct of the

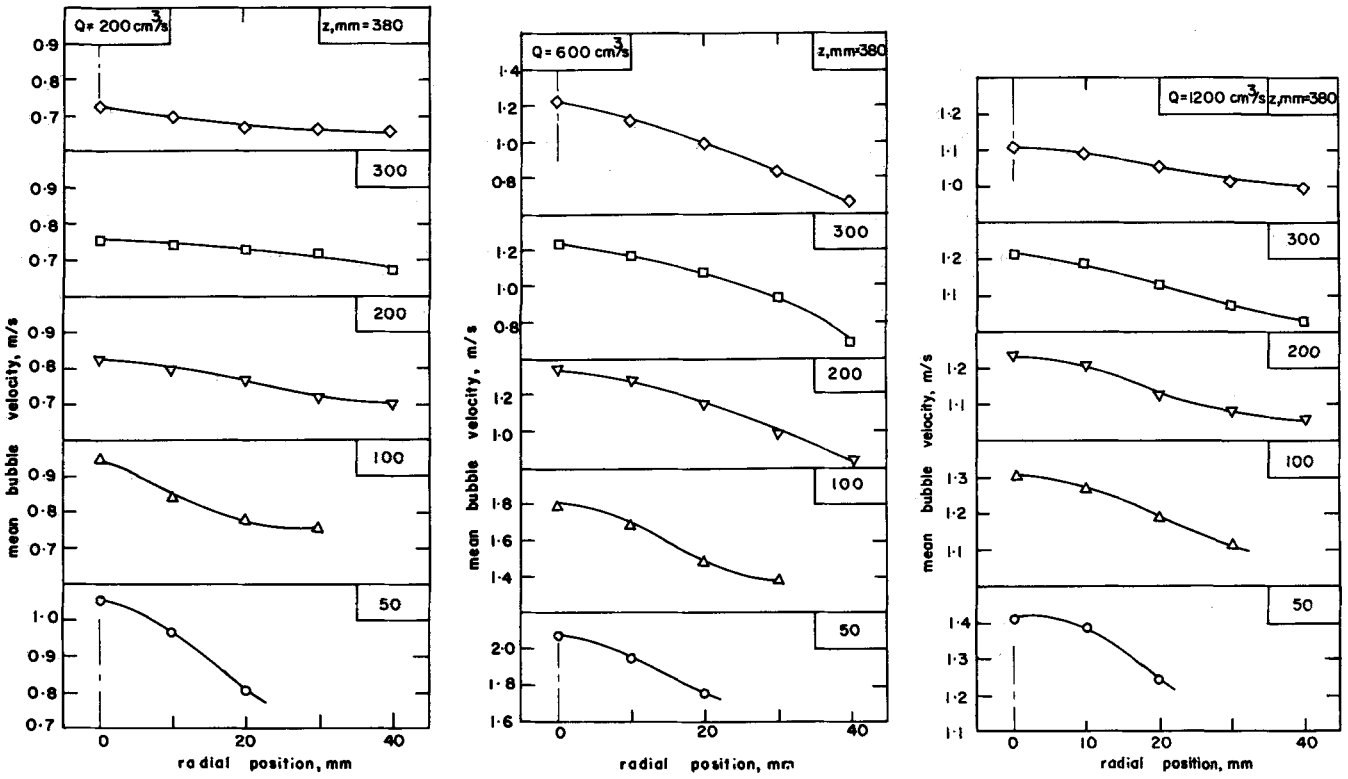

(*a*) (*b*) (*c*)

Fig. 10—Bubble velocity profiles: (*a*) 200 cm³/s, (*b*) 600 cm³/s, and (*c*) 1200 cm³/s.

corresponding value at 600 cm³/s. The decrease can be attributed to the increased resistance of the liquid phase to the initial motion of the large envelope resulting from coalescence, as well as the loss in kinetic energy of the gas in the process of coalescence, with turbulent circulation in the envelope.[29] As from the height of about 100 mm above the plug, the bubble rise velocities at 1200 cm³/s become nearly equal to the corresponding values at 600 cm³/s, following the gradual breakdown of the large envelope into smaller gas packets mixed with the tiny discrete bubbles.

E. *Bubble Size Distribution*

The mean axial bubble diameters at various heights above the plug are shown in Figure 11 for the three values of gas flow rate. At 200 cm³/s, which is in the discrete bubble regime, the bubble diameter decreases, but very slightly with height, from about 4 mm at 50 mm above the plug to about 3 mm at the upper regions of the plume. With incipient coalescence at 600 cm³/s, the mean bubble size increases significantly to about 35 mm at 50 mm above the plug but also drops rapidly with increasing height to about 20 mm at the height of 380 mm. A similar trend is observed at 1200 cm³/s when there is full coalescence at the plug; the mean axial bubble size is as much as 50 mm close to the plug, dropping sharply with height to about 22 mm toward the surface of the bath.

It is interesting to compare these results with the measurements of bubble pierced length (axial diameter) made

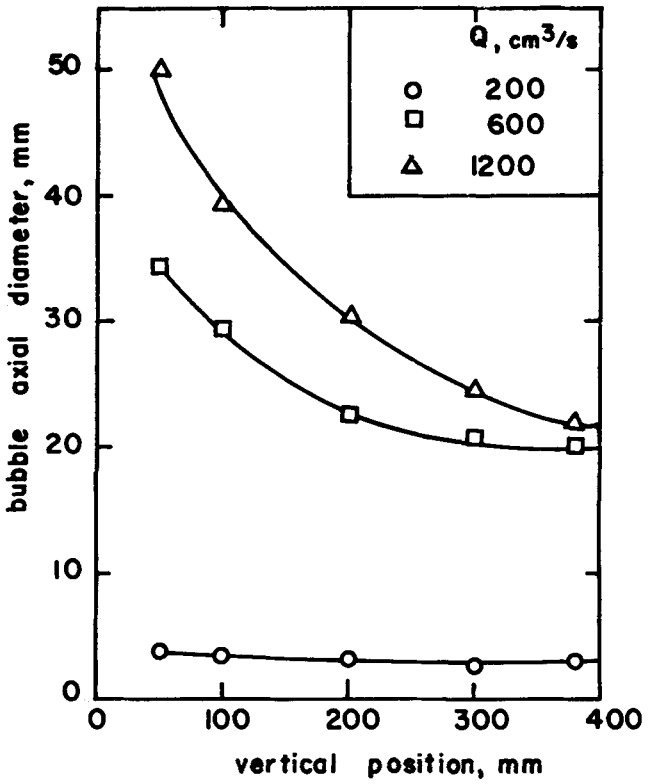

Fig. 11—Axial bubble diameter distribution.

by Castillejos and Brimacombe[24] for the case of tuyere injection. For the same depth of liquid (400 mm) and orifice diameters of 4.10 and 6.35 mm, the bubble pierced length stabilizes at 15 mm beyond the height of about 120 mm above the orifice over a range of gas flow rates between 371 and 1257 cm^3/s. Thus, the porous plug operating in the discrete bubble regime produces bubbles four to five times smaller in diameter than could be found in the fully developed plume above the tuyere. On the other hand, once coalescence has started at the porous plug, the resultant gas envelopes do not break down as rapidly as in the case of the tuyere, and relatively larger bubbles persist to the surface of the porous plug plume. This observation supports the idea that the disintegration of the bubble formed at an orifice is largely precipitated by the turbulent wake created by the bubble itself.[30] Turbulence in porous plug injection is limited by the large pressure drop across the plug, and hence, any large bubbles resulting from coalescence at the plug tend to be more stable in their rise through the liquid than bubbles formed at the plate orifice.

By implication, the effectiveness of the porous plug in gas-liquid contacting lies more in its ability to produce fine bubbles with increased overall surface area than in the mixing power of the injection. It is therefore important that the plug is operated under conditions of discrete bubble formation; otherwise, the performance under conditions of coalescence could even be inferior to the plain tuyere. It has indeed been shown experimentally that the porous plug rapidly loses its superiority over the tuyere with increasing gas flow rate in the absorption of carbon dioxide into sodium hydroxide.[15]

F. *Liquid Velocity Profiles*

The liquid velocities were measured in the annular region surrounding the plume from a radial distance of 50 mm outward to 200 mm (*i.e.*, 50 mm from the wall of the tank). Measurements could not be made closer to the plume due to the interference of fine gas bubbles with the styrene seedings in the liquid phase, leading to spurious data from the velocimeter. Measurements were made for both axial and radial velocity components at five different levels in the liquid phase and for the three different gas flow rates.

1. *Axial liquid velocity components*

The radial distributions of the axial liquid velocities are shown in Figure 12. In the regimes of discrete bubbles and incipient coalescence, the distributions are consistently nearly sigmoidal. Above the height of 50 mm with respect to the plug surface, the axial liquid velocities are relatively high close to the plume but decrease rapidly between the radial distances of 50 and 100 mm. At all levels, the velocities decrease more gradually beyond the radial distance of 100 mm, becoming negative (*i.e.*, downward) beyond about 170 mm from the axis of the plug.

It can be seen from Figure 12 that the axial liquid velocities generally increase with increasing height above the plug. This can be explained by the pumping action of the plume, which gradually accelerates the liquid phase upward. In the discrete bubble regime, for instance, the axial liquid velocity at 200 cm^3/s and a radial distance of 50 mm increases from about 0.06 m/s at the height of 50 mm to about 0.38 m/s at 380 mm. Similarly, with

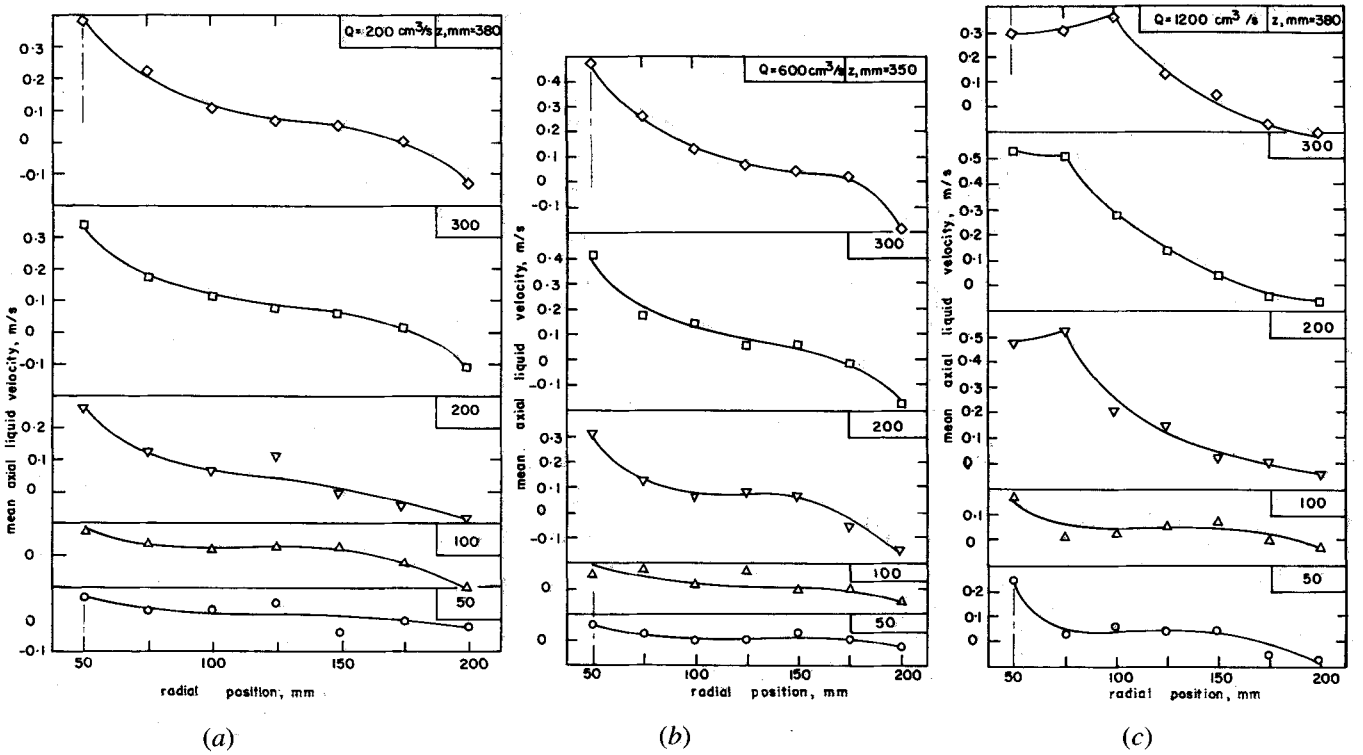

Fig. 12—Axial liquid velocity profiles: (*a*) 200 cm^3/s, (*b*) 600 cm^3/s, and (*c*) 1200 cm^3/s.

incipient coalescence, the corresponding velocities at 600 cm^3/s are 0.06 m/s at 50 mm, increasing to 0.48 m/s at 380 mm. The downward axial velocities of the liquid toward the sides of the tank also show a similar trend. Thus, at a gas flow rate of 200 cm^3/s and radial distance of 200 mm, the axial liquid velocity varies from about −0.13 m/s at 380-mm height to −0.02 m/s at 50-mm height. The corresponding values at 600 cm^3/s are −0.18 and −0.03 m/s.

The axial velocity profiles in the coalescence regime only show the sigmoidal distribution at low levels, up to about 100 mm above the plug. In the higher regions, the velocities do not appear to be increasing toward an axial peak; they tend to flatten out from a radial distance of 75 to 100 mm, toward the axis of the plug. This feature can be attributed to the high degree of turbulence which is manifested at the high injection rates and particularly in the upper sections of the bath. It is probably related to the "double-peak" effect reported by Kawakami *et al.*[31] in tuyere injection.

2. *Radial liquid velocity profiles*

The radial liquid velocities shown in Figure 13 are designated positive when the flow is outwards, from the axis of flow toward the walls of the tank. In general, the radial velocities are much lower than the corresponding axial components, especially toward the periphery of the plume. It was also observed, from more data than could clearly be shown in Figure 13, that the radial flow of liquid was generally outward (positive) from a height of about 340 mm above the plug, irrespective of the gas injection rate; below this level, from the walls toward the plug, the flow was negative. Considered along with

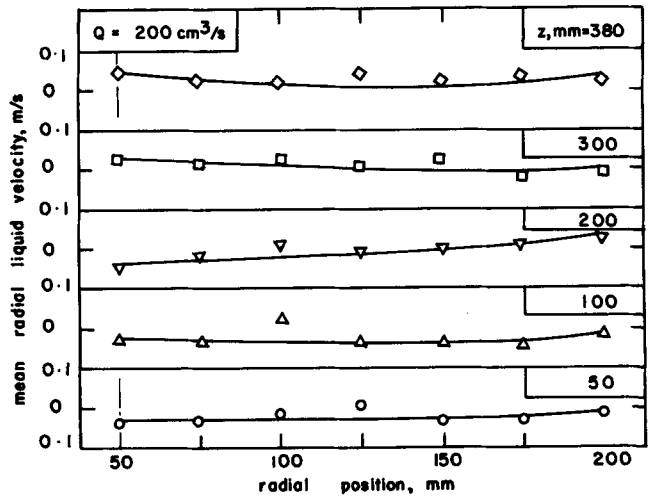

(*a*)

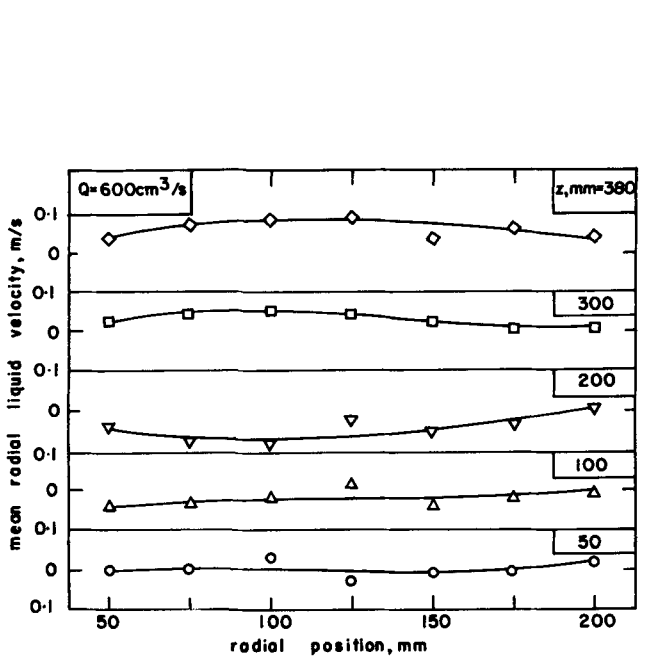

(*b*)

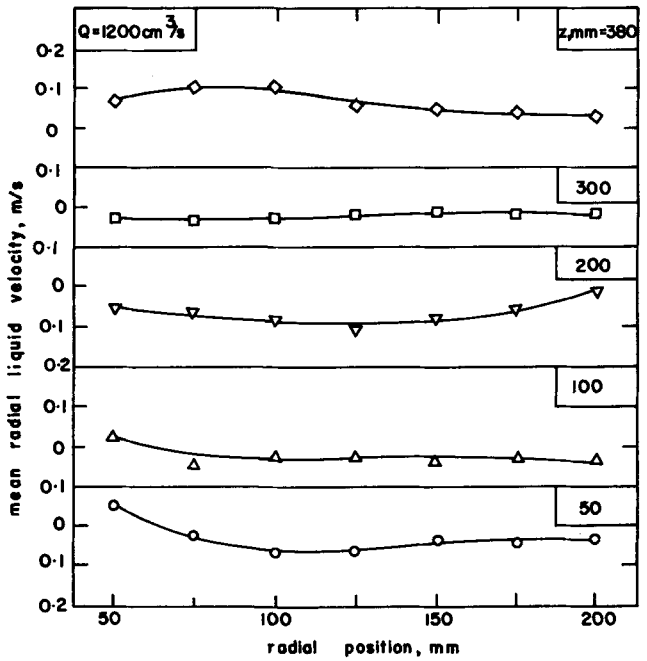

(*c*)

Fig. 13—Radial liquid velocity profiles: (*a*) 200 cm^3/s, (*b*) 600 cm^3/s, and (*c*) 1200 cm^3/s.

the similar change in direction of the axial liquid flow at a radial distance of about 170 mm, a clear picture emerges in Figure 14 of the usual convection mixing currents associated with gas-stirred liquid tanks.

The positive radial velocities increase slightly with increasing height toward the surface, but there is no definite pattern of variation with radial distance at the different levels considered. It has already been pointed out that laser beams projected close to the static surface of the bath were deflected by surface waves, making it impossible to measure the radial velocities in that region where visual observations indicate that the values could be substantial. In general, the positive radial velocities also increase slightly with gas injection rate, the maximum recorded value of about 0.1 m/s occurring at 1200 cm^3/s, at the height of 380 mm above the plug.

IV. SUMMARY AND CONCLUSIONS

Experimental measurements in a 1/6th-scale air-water model of a 150-tonne ladle equipped with a porous plug show three modes of gas dispersion in the bath; fine discrete bubbles are formed up to a specific gas flow rate of about 14 $cm^3/s\ cm^2$ up to the plug surface, followed by incipient coalescence, which then becomes fully established beyond 40 $cm^3/s\ cm^2$. In all dispersion regimes, the gas fraction profiles are bell-shaped, with the gas fraction increasing with increasing gas flow rate but decreasing height above the plug and radial distance from the plug axis. Thus, the axial values of the gas fraction are well correlated by means of the reduced height above the plug. The bubble frequency profiles are also consistently bell-shaped; the frequency increases with decreasing height and increasing gas flow rate but drops off with the onset of bubble coalescence. The reduced frequencies and gas fractions are close to Gaussian functions of the reduced radial distance from the axis of flow. The bubble velocity profile, which is also symmetrical about the axis, increases with increasing gas injection rate but decreases with increasing height, radial distance, and like the frequency, as soon as coalescence is established. The bubbles are fine, between 3 and 4 mm in diameter, in the discrete bubble regime but become larger on the average (35 to 50 mm) deep in the bath in the event of coalescence. Bubble disintegration is slow compared with the tuyere, and hence, it is vital to ensure that porous plugs operate in the discrete bubble regime to be most effective. In the liquid phase surrounding the plume, the axial velocity profile is sigmoidal, with the values increasing with increasing height above the plug but decreasing with increasing radial distance. Indeed, the flow reverses from upward to downward beyond a radial distance of about 170 mm from the plug axis at all flow rates considered. The corresponding radial velocity components are relatively small and increase slightly with increasing height and flow rate. There is also a reversal in flow, from radially outward toward the bath surface to radially inward, below the height of about 340 mm. The axial and radial flow reversals clearly identify the convection flow pattern in the bath.

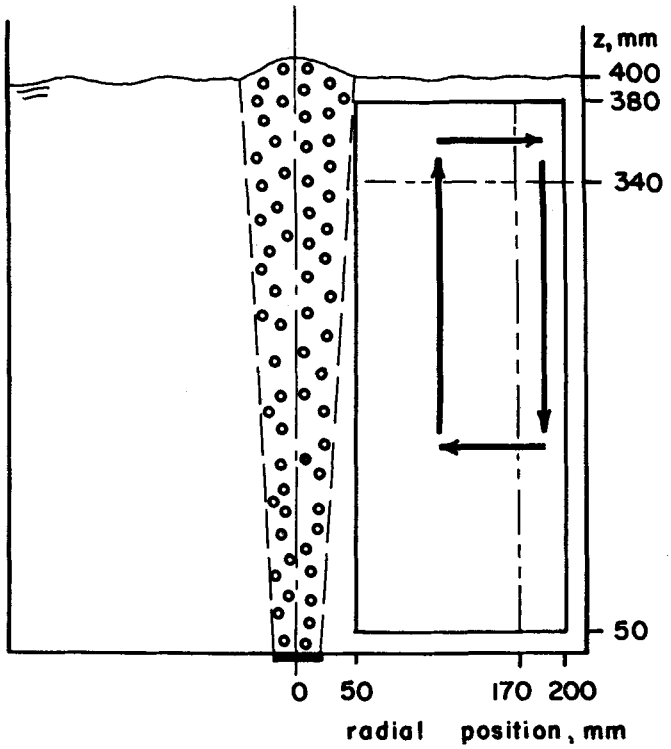

Fig. 14—Liquid circulation pattern in porous plug injection.

NOMENCLATURE

A	cross-sectional area of the porous plug, mm^2
C	constant for plume velocity correlation in Eq. [6]
d	average bubble diameter, mm
f	bubble frequency, s^{-1}
f_0	axial bubble frequency, s^{-1}
Fr	Froude number, $u^2/\varepsilon^2 g\delta$
g	acceleration due to gravity (981 m/s^2)
h	height of the porous plug, mm
K	coefficient for bubble diameter in Eq. [3]
L	liquid depth, mm
n	exponent for bubble diameter in Eq. [3]
ΔP	pressure drop across the plug, $g/cm\ s^2$
ΔP_f	frictional component of the pressure drop, $g/cm\ s^2$
Q	gas flow rate, cm^3/s
R	radius of tank, mm
r	radial distance from plug axis, mm
$r_{\alpha_0/2}$	gas fraction half-value radius, mm
$r_{f_0/2}$	bubble frequency half-value radius, mm
u	superficial gas velocity, m/s
U_p	plume velocity, m/s
We	Weber number, $u^2\delta\rho/\varepsilon^2\sigma$
z	height above the plug, mm
α	gas fraction
α_0	axial gas fraction
δ	pore diameter, mm
ε	plug porosity
ρ	liquid density, g/cm^3
ν	kinematic viscosity of the gas, cm^2/s
ζ	permeability of the plug, cm^5/g

ACKNOWLEDGMENTS

This work was supported by funds from the CIDA/NSERC Research Associateships Program when one of the authors (P.E. Anagbo) was on study leave at the University of British Columbia.

REFERENCES

1. P.E. Anagbo and J.K. Brimacombe: *I&SM Iron Steelmaker*, 1988, Oct., pp. 38-43.
2. P.E. Anagbo and J.K. Brimacombe: *I&SM Iron Steelmaker*, 1988, Nov., pp. 41-45.
3. B.A. Strathdee and D.M. McFarlane: *Iron Steel Eng.*, 1971, vol. 48, pp. 82-87.
4. S.L. Peck: *Steelmaking Conf. Proc.*, ISS-AIME, 1981, vol. 64, pp. 284-87.
5. Y. Suzuki and T. Kuwabara: *Ironmaking and Steelmaking*, 1978, vol. 2, pp. 80-88.
6. K. Upadhya: *J. Met.*, 1983, vol. 35, pp. 32-36.
7. N.J. Themelis and P. Goyal: *Can. Metall. Q.*, 1983, vol. 22, pp. 313-20.
8. B. Grabner and H. Hoeffgen: *Radex Rundschau*, 1985, vol. 3, pp. 581-610.
9. S.A. Sholl: *Mod. Cast.*, 1968, vol. 53, pp. 73-76.
10. G. McGlothlin: *Trans. Am. Foundrymen's Soc.*, 1978, vol. 85, pp. 5-8.
11. K. Mori: *Imono*, 1982, vol. 54, pp. 55-56.
12. P. Goyal, N.J. Themelis, and W.A. Zanchuk: *J. Met.*, 1982, vol. 34, pp. 28-38.
13. G. Goyal, S.V. Joshi, and J. Wang: *J. Met.*, 1983, vol. 35, pp. 52-58.
14. C.W. Booth and A.J. Clegg: *Br. Foundryman*, 1984, vol. 77, pp. 96-106.
15. T. Stapurewicz and N.J. Themelis: *Can. Metall. Q.*, 1987, vol. 26, pp. 123-28.
16. G. Houghton, A.M. McLean, and P.D. Ritchie: *Chem. Eng. Sci.*, 1957, vol. 7, pp. 40-50.
17. K. Koide, S. Kato, Y. Takana, and H. Kubota: *J. Chem. Eng. Japan*, 1968, vol. 1, pp. 51-56.
18. R.T. Baxter and A.E. Wraith: *Chem. Eng. Sci.*, 1970, vol. 25, pp. 1244-47.
19. S.T. Johansen, D.G.C. Robertson, K. Woje, and T.A. Engh: *Metall. Trans. B*, 1988, vol. 19B, pp. 745-54.
20. S.T. Johansen and F. Boysan: *Metall. Trans. B*, 1988, vol. 19B, pp. 755-64.
21. Y. Sahai and R.I.L. Guthrie: *Metall. Trans. B*, 1982, vol. 13B, pp. 193-202.
22. Y. Sahai and R.I.L. Guthrie: *Metall. Trans. B*, 1982, vol. 13B, pp. 203-11.
23. T. Stapurewicz and N.J. Themelis: *Can. Metall. Q.*, 1987, vol. 26, pp. 123-28.
24. A.H. Castillejos and J.K. Brimacombe: *Metall. Trans. B*, 1987, vol. 18B, pp. 649-58.
25. F. Durst, A. Melling, and J.H. Whitelaw: *Principles and Practices of Laser-Doppler Anemometry*, Academic Press, London, 1976.
26. D.R.J. Owen and F. Hinton: *A Simple Guide to Finite Elements*, Pineridge Press, Swansea, Wales, 1980.
27. K.-H. Tacke, H.-G. Schubert, D.-J. Weber, and K. Schwerdtfeger: *Metall. Trans. B*, 1985, vol. 16B, pp. 263-75.
28. A.E. Wraith and T. Kakutani: *Chem. Eng. Sci.*, 1974, vol. 29, pp. 1-12.
29. P.E. Anagbo: *Can. J. Chem. Eng.*, 1980, vol. 60, pp. 220-25.
30. P.E. Anagbo, J.K. Brimacombe, and A.H. Castillejos: *Int. Symp. on Ladle Steelmaking and Furnaces*, CIM, Montreal, PQ, 1988, pp. 29-46.
31. M. Kawakami, Y. Kitazama, T. Nakamura, T. Miyake, and K. Ito: *Trans. ISIJ*, 1985, vol. 25, pp. 394-402.